ACS APPLIED MATERIALS & INTERFACES

www.acsami.org
Research Article

Large Biaxial Compressive Strain Tuning of Neutral and Charged Excitons in Single-Layer Transition Metal Dichalcogenides

Eudomar Henríquez-Guerra, Hao Li, Pablo Pasqués-Gramage, Daniel Gosálbez-Martínez, Roberto D'Agosta, Andres Castellanos-Gomez,* and M. Reyes Calvo*

Cite This: https://doi.org/10.1021/acsami.3c13281

ABSTRACT: The absorption and emission of light in single-layer transition metal dichalcogenides are governed by the formation of excitonic quasiparticles. Strain provides a powerful technique to tune the optoelectronic properties of two-dimensional materials and thus to adjust their exciton energies. The effects of large compressive strain in the optical spectrum of two-dimensional (2D) semiconductors remain rather unexplored compared to those of tensile strain, mainly due to experimental constraints. Here, we induced large, uniform, biaxial compressive strain (~1.2%) by cooling, down to 10 K, single-layer WS_2, MoS_2, WSe_2, and $MoSe_2$ deposited on polycarbonate substrates. We observed a significant strain-induced modulation of neutral exciton energies, with blue shifts up to 160 meV, larger than in any previous experiments. Our results indicate a remarkably efficient transfer of compressive strain, demonstrated by gauge factor values exceeding previous results and approaching theoretical expectations. At low temperatures, we investigated the effect of compressive strain on the resonances associated with the formation of charged excitons. In WS_2, a notable reduction of gauge factors for charged compared to neutral excitons suggests an increase in their binding energy, which likely results from the effects of strain added to the influence of the polymeric substrate.

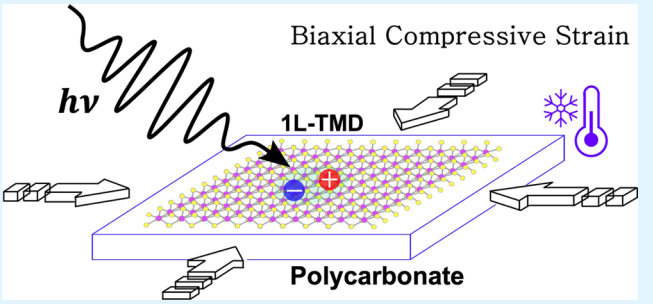

KEYWORDS: *2D materials, transition metal dichalcogenides, biaxial compressive strain, micro-reflectance spectroscopy, differential reflectance, excitons, trions, binding energy*

INTRODUCTION

Two-dimensional (2D) semiconductors possess unique electronic, optical, and optoelectronic properties. In particular, at the single-layer limit (1L), transition metal dichalcogenides (TMDs) exhibit a direct-bandgap electronic structure which is favorable for light emission.[1,2] Additionally, the increased strength of Coulomb interactions at the single layer limit results in the formation of exciton bound states with large binding energies—up to hundreds of meV.[3,4] This leads to robust excitonic light absorption and emission even at room temperature, making 2D-TMDs candidate materials for the design of ultrathin, flexible optoelectronic devices.[1,3,5−8] Very recently, excitons in 2D semiconductors have been proposed to transmit information with low energy dissipation in the so-called excitonic devices.[9−11] Furthermore, the manipulation of excitonic coherent states in single-layer TMDs has been proposed as a platform for quantum information technologies.[4,12−14]

In addition to their exceptional optical and mechanical properties, single-layer semiconductors exhibit a remarkable tunability in their electronic and optoelectronic properties.[15−17] Strain has been widely recognized as a very effective tool for tuning the properties of 2D materials.[18−22] For instance, strain modifies the electronic band structure of single- and few-layer TMD semiconductors, increasing or decreasing their band gap energy if the applied strain is either compressive or tensile.[21] This, in turn, determines their optical spectra, modulating exciton energies.[22,23] In fact, strain-induced changes in the electronic structure of TMDs have been extensively studied by tracking the shift in energy of excitonic emission or absorption using photoluminescence or reflectance spectroscopy measurements.[24−29]

Large amounts of uniform tensile strain, both uniaxial and biaxial, have been successfully induced in 2D semiconductors by bending them on flexible substrates.[6,7,24,27,30−32] For instance, uniaxial strain up to ~2.8% has been achieved in 1L-MoS_2[24,30] and gauge factors for excitons up to 100 meV/% have been demonstrated for biaxial strain.[27] The effects of larger, nonuniform, biaxial tensile strain on the optical

Received: September 5, 2023
Revised: November 16, 2023
Accepted: November 17, 2023

properties of TMDs have also been explored by nanoindentation methods[26] and by pressurizing single-layer membranes.[29,33] Some of these methods have also been applied to explore the impact of tensile strain on the binding energies and valley selectivity of excitonic species in single-layer TMDs.[34−36] However, experimental methods to apply compressive strain and to study its effects on the properties of 2D materials are limited. Apart from hydrostatic pressure techniques,[28] piezoelectric actuators have been recently employed to transfer modest amounts of purely biaxial compressive strain (~0.3%).[37,38] An alternative method for generating larger, homogeneous, biaxial compressive strain involves transferring it from substrates with large thermal expansion coefficients. This approach enables strain modulation through sample temperature control and has been recently applied to strain engineering of 2D materials.[39−43] For instance, the effect of compressive strain in the photoresponse of MoS_2 on polycarbonate has been investigated by cooling down to 80 K.[39]

In this work, we achieve large, reproducible amounts of uniform biaxial compressive strain, up to ca. −1.2% in single-layer TMDs. Strain is transferred from a polymer substrate, polycarbonate (PC), with a large thermal expansion coefficient during the cooling process from 300 to 10 K. To determine the effect of compressive strain, we compare the evolution of exciton resonances with temperature in single-layer TMD samples deposited on PC with similar ones on Si/SiO_2 (substrate with negligible thermal expansion coefficient). When cooling down, we observe a significantly larger energy blue shift of the exciton resonances for samples on PC compared to samples on Si/SiO_2 substrates, which we attribute to the strain transferred from the compression of the polymer substrate. From the comparison of exciton energy shifts for samples on both substrates, we determine strain gauge factors for neutral excitons in single-layer WS_2, MoS_2, WSe_2, and $MoSe_2$ under uniform biaxial compressive strain. Our results indicate an excellent transfer of strain to the single-layer TMDs, with exciton energy shifts and gauge factor values that substantially surpass the best results from previous compressive strain experiments. Furthermore, in the low-temperature regime, we reach a situation that combines high levels of biaxial compressive strain with enhanced spectroscopic resolution. This allows us to resolve additional resonances, which we associate with the formation of charged excitons (trions) in 1L-MoS_2 and 1L-WS_2. Strain gauge factors for trions are similar to those for neutral excitons in 1L-MoS_2, but smaller in 1L-WS_2. This suggests an increase in the binding energy of trions with strain in 1L-WS_2, which we discuss in terms of simplified models. We conclude that the large trion binding energy (~80 meV) observed in strained 1L-WS_2 likely originates from the combination of the substrate influence and the strain-induced changes in the electronic properties of the material.

RESULTS AND DISCUSSION

Single-layer samples of WS_2, MoS_2, WSe_2, and $MoSe_2$ were deposited on polycarbonate substrates (see ref 44 and the Materials and Methods section). Their thickness was confirmed by the energy position of exciton resonances in the differential reflectance spectra (Figure 1a), following ref 45, and by Raman spectroscopy (Supporting Information Section S1). Polycarbonate (PC) presents both a large Young modulus ($E \sim 2.5$ GPa)[25] and a large thermal expansion coefficient at

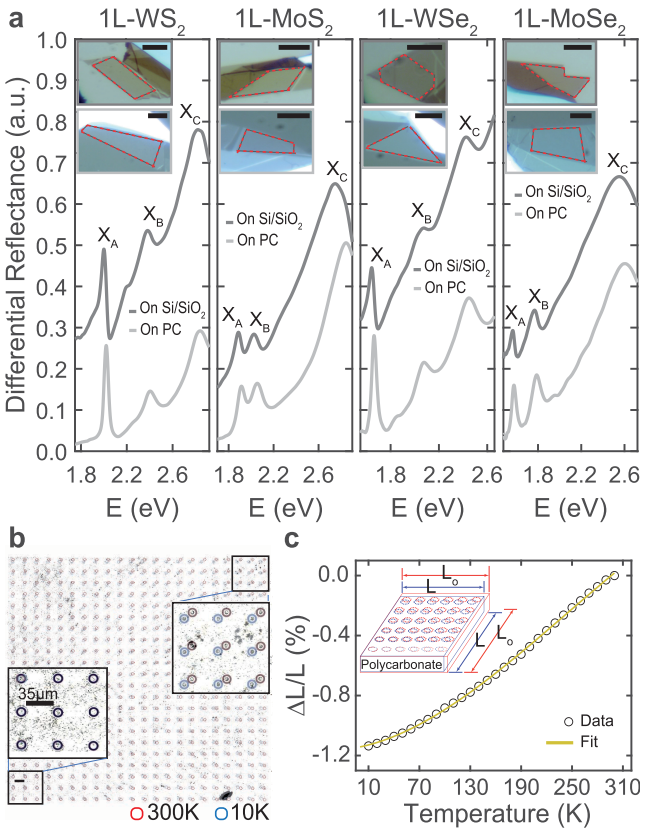

Figure 1. (a) Differential reflectance spectroscopy of single-layer samples of WS_2, WSe_2, MoS_2, and $MoSe_2$ on Si/SiO_2 (dark gray) and polycarbonate (light gray) substrates. The differential reflectance is calculated as $(R_{substrate} - R_{sample})/R_{substrate}$ for samples on Si/SiO_2 and as $(R_{sample} - R_{substrate})/R_{substrate}$ for samples on PC, to enable a clear comparison between data obtained for samples on the two substrates. Data are shifted for clarity. The insets show optical images of the samples, where the single-layer area is marked with a dotted red line. Scale bars represent 10 μm. (b) Optical images of a resist micropillars grid (~13 um of diameter) on a polycarbonate substrate at 300 and 10 K. The contrast of images has been adjusted to enhance the visibility of the micropillar positions. The perimeter of each micropillar is depicted in red for 300 K and in blue for 10 K. (c) Average percentage decrease in the distance between pillars as the temperature is lowered, measured from images similar to those in (b) taken at 10 K intervals ranging from 300 to 10 K. The solid line represents a fitting of data to a polynomial function.

room temperature ($\alpha \sim 6.5 \times 10^{-5}$ K^{-1}),[39] making it an ideal candidate substrate for strain transfer.[39,40] To isolate the effect of strain from temperature, we prepared similar samples on Si/SiO_2 substrates, a material with 2 orders of magnitude lower thermal expansion coefficient ($\alpha \sim 5 \times 10^{-7}$ K^{-1}).[46] Figure 1a presents optical images and differential reflectance spectroscopy for single-layer samples of WS_2, MoS_2, WSe_2, and $MoSe_2$ transferred both on PC and on Si/SiO_2 (the thickness of the SiO_2 layer is 50 nm) substrates at room temperature under ambient conditions. The spectra exhibit distinct asymmetric resonances corresponding to three different species of excitons (X_A, X_B, X_C). The different resonance shapes observed on the two substrates may stem from constructive interference effects at Si/SiO_2, along with the broadening of the resonances on PC, which is likely the result of PC being comparatively less flat and homogeneous as a substrate than SiO_2. An energy difference of ca. 10−20 meV is also observed between exciton

https://doi.org/10.1021/acsami.3c13281
ACS Appl. Mater. Interfaces XXXX, XXX, XXX−XXX

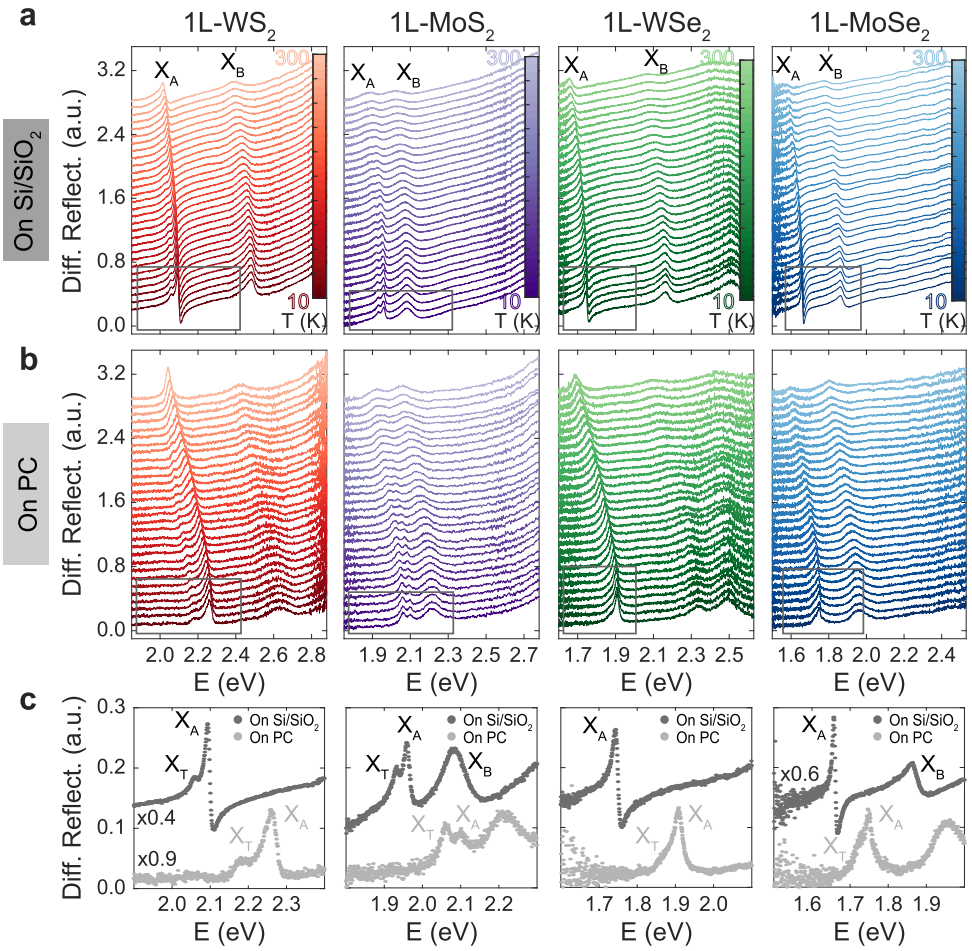

Figure 2. (a, b) Differential reflectance as a function of temperature for single-layer TMD samples on (a) Si/SiO_2 and (b) polycarbonate (PC) substrates. Data corresponding to each single-layer material (WS_2, MoS_2, WSe_2, and $MoSe_2$) are accordingly labeled at the top row of the figure. Data are vertically shifted for clarity. (c) Comparison of differential reflectance spectra obtained at base temperature (10 K) for samples on Si/SiO_2 and PC substrates, respectively, zooming into the X_A resonance energy range, which is marked with a gray line rectangle in (a) and (b).

resonances of the same 1L-TMD on Si/SiO_2 and PC substrates. The dielectric constant of PC ($\varepsilon_r \sim 2.3–2.8$[47,48]) being smaller than that of SiO_2 ($\varepsilon_r \sim 3.9$[49]), may result in different energy values for excitons in samples on PC compared to those on Si/SiO_2. This variation stems from changes in the bandgap and exciton binding energies due to the different dielectric environments.[16,50]

Prior to studying the temperature-dependent optical properties of the 1L-TMD samples, the thermal compression of polycarbonate from 300 to 10 K was quantified by applying the method proposed in refs 39,40. Photoresist micropillars were patterned on top of a polycarbonate substrate (Figure 1b,c). The distance L between two pillars located at diagonally opposite corners of the image area in Figure 1b was tracked as a function of temperature. The thermal compression of the polycarbonate sample was determined as $\Delta L/L = (L - L_0)/L_0$, where L_0 is the distance in the uncompressed PC measured at room temperature. $\Delta L/L$ quantifies the compression level of the PC substrate and means the maximum strain that can be transferred to the 1L-TMDs on top of it. Compression increases down to 150 K and, below that, the compression rate decreases, reaching ~1.2% at 10 K, in agreement with ref 51. A fit to a polynomial expression will be used to correlate substrate compression and temperature $\frac{\Delta L}{L}(\%) = -2.1 \times 10^{-8}T^3 + 1.5 \times 10^{-5}T^2 + 1.2 \times 10^{-3}T - 1.14$.

Next, we compare variable-temperature micro-reflectance measurements on TMD single layers on PC and on Si/SiO_2—substrate with negligible thermal compression coefficient (see the Materials and Methods section and Supporting Information Section S2). The temperature evolution of the differential reflectance is presented in Figure 2a for single layers of four different TMDs (1L-WS_2, 1L-MoS_2, 1L-WSe_2, and 1L-$MoSe_2$). At room temperature, two resonances are visible in all four materials, corresponding to the A and B excitons, labeled X_A and X_B in Figure 2a. These spectra are taken under vacuum conditions ($P < 10^{-6}$ mbar) and an energy shift of ~20 meV in the energy positions of X_A and X_B is observed when compared to the ambient spectra in Figure 1. This shift is likely due to the absence of adsorbents that affect the dielectric environment.[15]

As temperature decreased, on Si/SiO_2 substrates, the exciton peaks of all four single-layer TMDs shifted toward higher energies. This trend follows the expected increase of the bandgap energy due to the freezing of electron–phonon interactions and the slight change in bonding lengths.[52,53] On Si/SiO_2 substrates, we attribute this shift to the sole effects of temperature, considering substrate deformation negligible. Notably, for samples on PC substrates, a significantly larger blue shift of X_A and X_B peaks with decreasing T was observed compared to samples on Si/SiO_2. We attribute the extra energy

https://doi.org/10.1021/acsami.3c13281
ACS Appl. Mater. Interfaces XXXX, XXX, XXX−XXX

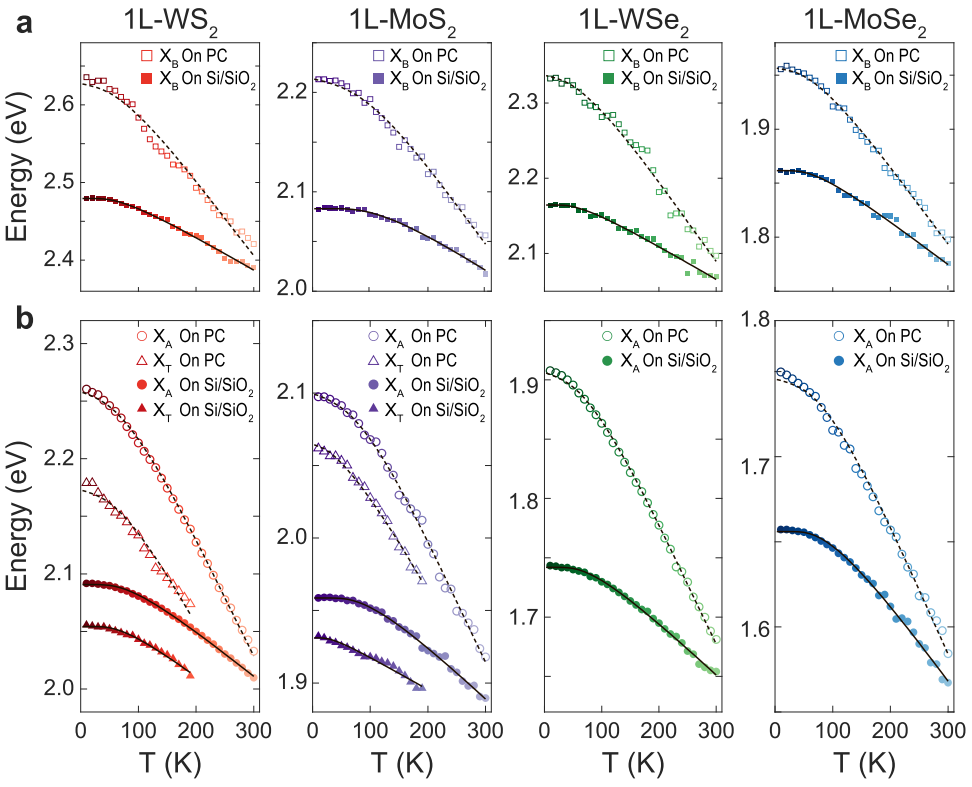

Figure 3. (a, b) Data points representing the energy positions for resonances (a) X_B and (b) X_A and X_T extracted from data in Figure 2 for 1L-WS_2, 1L-MoS_2, 1L-WSe_2, and 1L-$MoSe_2$, on Si/SiO_2 and PC substrates, respectively. In the case of data on Si/SiO_2 substrates, solid lines represent the fit of data to the model for the bandgap energy evolution with temperature proposed in ref 52. In the case of samples on PC substrates, the dashed line represents the exciton energy evolution estimated from the addition of the effect of strain (calculated later in the article from the analysis in Figure 4) to the effect of temperature. The effects of temperature are estimated from the fitting to the bandgap model for data in the same material on a Si/SiO_2 substrate.

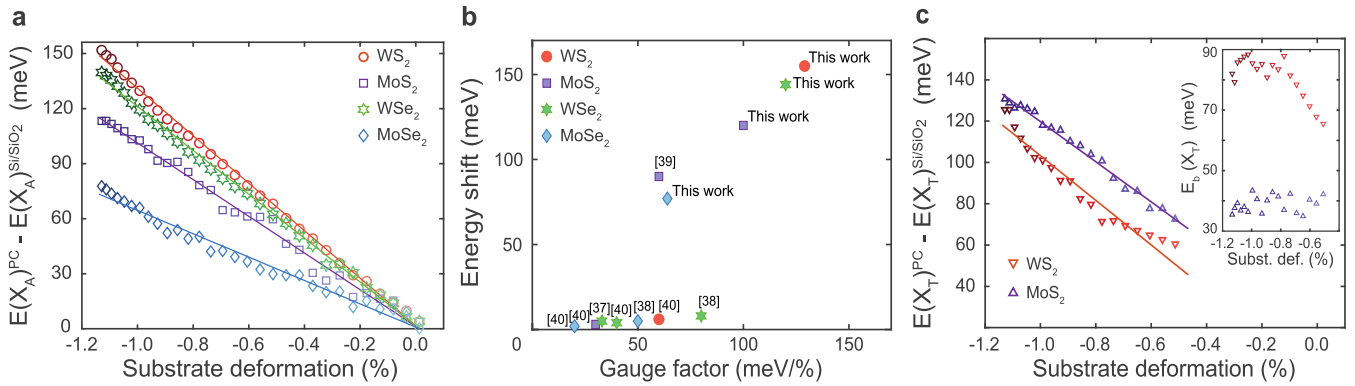

Figure 4. (a, c) Data points represent the energy difference $\Delta E(X) = E_X^{PC} - E_X^{Si/SiO_2}$ between (a) X_A excitons and (c) X_T charged excitons on the two different substrates, PC and Si/SiO_2, as a function of substrate deformation (estimated as $\Delta L/L$ in Figure 1c), for a single layer of each of the four materials under study. In (a), the exciton energy difference between substrates at room temperature has been subtracted from the data for clarity (see Supporting Information Section S6). Solid lines represent linear fits to the data. The slope of these linear fits yields the gauge factors presented in Table 1. (b) Comparison of the maximum energy blueshift of the bandgap energy and gauge factor values obtained in this work with those from other works on biaxial compressive strain.[37−40] The bandgap energy shift is assumed to be the same as for X_A when it applies. For a fair comparison, the effect of temperature has been removed in other thermal compression experiments using the same method applied to our data. The inset in (c) shows the energy difference between X_T and X_A, associated with the binding energy of a negatively charged exciton, $E_b(X_T) = E(X_T) - E(X_A)$, for 1L-$MoS_2$ and 1L-WS_2 on PC.

shift observed for samples on PC to the strain transferred to the 1L-TMDs from the thermal compression of the PC substrate.[40] At low temperatures, as the width of the resonances decreases, a peak can be resolved at energies lower than those of exciton *A*. This peak is more pronounced in the 1L-MoS_2 and 1L-WS_2 spectra for both Si/SiO_2 and PC substrates (Figure 2c), where it clearly appears below 200 K. A shoulder on the left side of X_A also appears for 1L-WSe_2 and 1L-$MoSe_2$, but only in samples on PC and at the base temperature (Figure 2c). In previous works, a similar peak has been observed in the optical spectra of various 1L-TMDs and has been typically associated with the absorption or emission

https://doi.org/10.1021/acsami.3c13281
ACS Appl. Mater. Interfaces XXXX, XXX, XXX−XXX

Table 1. Strain Gauge Factors Obtained from the Slope of Exciton Energies versus Substrate Deformation in Figure 4[a]

Gauge factor (meV/%)	X_A this work	X_A theory	X_B this work	X_B theory	X_T this work
1L-WS_2	−129 ± 3	−151[40]	−112 ± 10	−130[40]	−108 ± 13
		−144.0[22]		−123.8[22]	
1L-MoS_2	−100 ± 3	−110[40]	−90 ± 5	−107[40]	−97 ± 3
		−112.5[22]		−109.8[22]	
1L-WSe_2	−120 ± 3	−134[40]	−129 ± 10	−111[40]	
		−131.2[22]		−109.7[22]	
1L-$MoSe_2$	−64 ± 4	−90[40]	−66 ± 4	−89[40]	
		−98.6[22]		−97.2[22]	

[a]Results are compared to theoretical predictions from refs 22,40.

from a negatively charged exciton, also known as a trion.[54−57] Given its resemblance to trionic resonances, we label this resonance X_T in Figure 2c.

The temperature evolution of the energy position of resonances X_A, X_B, and X_T (see Supporting Information Section S3 for details) is presented in Figure 3. For all four 1L-TMDs on Si/SiO_2 substrates, X_A and X_B energy positions can be fitted to a model that describes the temperature dependence of the bandgap energy[52] (solid lines in Figure 3, Supporting Information Section S4). For both 1L-MoS_2 and 1L-WS_2 on Si/SiO_2 substrates, X_T follows a trend similar to that of X_A (see Figure 3b) and fitting with the same bandgap model yields similar parameters as for X_A and X_B (see Supporting Information Section S4). This fact suggests that the blue shift of exciton energies—which are the difference between bandgap energy and exciton binding energy—is dominated by changes in the bandgap and that temperature appears to have no significant effect on the binding energies of the corresponding excitonic states. The effect of temperature-induced changes in the substrate dielectric screening can be also disregarded. According to ref 48, the dielectric constant of polycarbonate decreases ∼2% at cryogenic temperature. This variation may lead to changes of just a few meV in the exciton energies of 1L-TMDs.[16,50]

To separate the effects of strain and temperature, we compared the energy positions of exciton peaks on PC (E_X^{PC}) and the corresponding values for similar samples on Si/SiO_2 (E_X^{Si/SiO_2}). The energy difference between each resonance on the two substrates, $\Delta E(X) = E_X^{PC} - E_X^{Si/SiO_2}$, is presented as a function of substrate deformation in Figure 4 (as a function of T in Supporting Information Section S5). Assuming that Si/SiO_2 data compiles the effects of temperature, $\Delta E(X)$ represents the blue shift in the exciton energy owing to the strain transferred from the compression of the PC substrate. Indeed, we find that $\Delta E(X)$ follows an almost linear relationship with substrate deformation and thus, with the amount of transferred strain (Figure 4a), in agreement with previous experimental and theoretical works.[22,40,58] Fitting $\Delta E(X)$ versus substrate deformation to a linear expression (Figure 4a) yields experimental strain gauge factors—defined as the exciton energy shift due to 1% of substrate deformation—for excitons A and B, which are summarized in Table 1 (see Supporting Information Section S6 for more details). The uncertainty values presented in Table 1 are the statistical errors obtained from the linear regression of the data in Figure 4. Gauge factors obtained for different samples differ by up to ∼10 meV/% (see Supporting Information Section S7). The extracted gauge factor values for X_A follow the hierarchy WS_2 > WSe_2 > MoS_2 > $MoSe_2$, in agreement with refs 22,40. This hierarchy has been attributed to the specific effects of strain on the band structure of each material.[40]

It is important to note that experimental gauge factors are calculated for substrate deformation and not actual strain. Therefore, a larger value of the experimental gauge factor, a larger energy shift for a given amount of substrate deformation, implies a more efficient transfer or strain. In Figure 4b, we compare our results to previous works on compressive strain in 1L-TMDs, considering two figures of merit: experimental gauge factor values, which assess the efficiency of the strain transfer, and the maximum induced energy shift, proportional to the maximum degree of compressive strain achieved. The large gauge factor values obtained for X_A in our work point to an excellent transfer of compressive strain from PC substrates to 1L-TMDs. This efficient transfer of strain, together with the level of deformation achieved, results in larger modulations of exciton energy for all four materials than in any previous compressive strain experiments. On the one hand, our gauge factor values are of similar magnitude to those obtained from piezo-actuator experiments,[37,38] but the amount of deformation achieved in our experiments is an order of magnitude larger. On the other hand, we obtain a significantly more efficient transfer of strain than in previous thermal compression experiments, likely due to performing the experiments under vacuum and maintaining precise control of temperature change rates (see the Materials and Methods section). In fact, our gauge factor values are nearly twice as high as those reported in previous experiments involving thermally induced strain.[39,40] Furthermore, our gauge factor values are comparable to the best values achieved for biaxial tensile strain using bending techniques,[27,31,32] or pressurized membranes[23,29] (see Supporting Information Section S8 for a detailed comparison). Moreover, these values closely align with those predicted by ab initio calculations[22,40] (see Table 1). Gauge factor values obtained from different computational methods exhibit variations of up to 10 meV/%. Theoretical gauge factor values, calculated as the energy shift per % of actual strain, can be considered an upper bound for experimental results. Differences in the quantitative agreement between theoretical and experimental values for different materials likely arise from the addition of experimental and theoretical uncertainties.

To assess the validity of our approach in separating the effects of temperature and strain, we plot, with the dashed line in Figure 2, the result of adding the temperature evolution of exciton energies for Si/SiO_2 substrates (assumed as negligible strain) plus a linear term on strain with the gauge factor as the slope coefficient. The good agreement with the experimental data suggests that the sole effect of temperature is similar for samples on both substrates and that disregarding changes in substrate effects with temperature is a reasonable assumption.

https://doi.org/10.1021/acsami.3c13281
ACS Appl. Mater. Interfaces XXXX, XXX, XXX−XXX

Gauge factors for X_B are obtained from a similar analysis (see Supporting Information Section S6) and compared in Table 1 with the corresponding theoretical estimates. In general, gauge factor values obtained for X_B are, within a larger error range, similar to those obtained for X_A.

Finally, we focus on the evolution of X_T resonances with substrate deformation for the two materials, MoS_2 and WS_2, where this peak can be resolved. On Si/SiO_2 substrates, X_T undergoes a similar energy shift with temperature as X_A in both 1L-WS_2 and 1L-MoS_2 (Figures 2a and 3b; Supporting Information Section S4). On PC substrates, X_T in 1L-MoS_2 exhibits a similar energy blue shift as X_A (Figures 2b and 3a). However, in 1L-WS_2 on PC, X_T deviates from this trend and displays a significantly smaller blue shift compared to X_A as temperature decreases (Figures 2b and 3a). To quantify this observation, we estimate gauge factors for X_T using the same method applied previously for X_A (Figures 3b and 4c). For 1L-MoS_2 on PC, we obtain an X_T gauge factor that is approximately the same, within error, as that for X_A. However, the gauge factor obtained for X_T in the case of 1L-WS_2 on PC is ∼20 meV/% smaller compared to X_A. Before addressing the potential causes of this effect, we discuss the origin of the resonance X_T. For samples on Si/SiO_2 substrates, the resemblance of resonances with those in other works[54,56] suggests that X_T arises from trion formation. Moreover, the relative intensity of X_T versus X_A being higher for 1L-MoS_2 and 1L-WS_2 on PC than on Si/SiO_2 (see Supporting Information Section S3) is also compatible with a trion origin for X_T, since trion relative spectral weight is highly dependent on free-carrier density.[59] Single-layer MoS_2 and WS_2 are typically described as intrinsically n-type doped semiconductors, and their doping level is often altered by charge transfer from the substrate. An alternative origin for X_T from a strain-induced direct-to-indirect bandgap transition (see refs 22,23) can be ruled out. First, if X_T originated from the indirect gap, it would be expected to appear similarly in 1L-WSe_2 since the evolution of the band structure with strain is nearly identical for single-layer WSe_2 and WS_2.[22] Second, to further understand the origin of X_T, we performed similar experiments in 1L-WS_2 deposited on a different polymer−polypropylene (PP) substrate. For 1L-WS_2 on PP, we obtained X_A gauge factors that were close to those obtained on PC (see Supporting Information Section S9), indicating a comparable strain transfer. Interestingly, the X_T peak observed on PC was absent for 1L-WS_2 on PP. Since the intensity and energy position of trion resonances strongly depend on the doping level of 1L-TMDs, they may significantly differ from substrate to substrate.[56,57,60] Therefore, the observed changes for X_T between samples on different substrates point to its origin in the formation of a charged quasiparticle, ruling out neutral excitons and biexcitons as potential sources.

All of the above support a trionic origin for X_T in 1L-MoS_2 and 1L-WS_2. This could also be the origin of the X_T shoulder observed in 1L-WSe2 and 1L-MoSe2 spectra at base temperature (Figure 2c), which could also stem from a higher doping level for these materials on PC compared to Si/SiO_2. However, in 1L-WSe_2 and 1L-$MoSe_2$, X_T resonances cannot be resolved at higher temperatures, limiting the study of their evolution with strain. We therefore focus on the investigation of strain effects for charged excitons in 1L-MoS_2 and 1L-WS_2. The energy difference between X_A and X_T, $E_b^T = E(X_A) - E(X_T)$, represents the binding energy of trions. This quantity remains approximately constant with temperature for both 1L-MoS_2 and 1L-WS_2 on Si/SiO_2, around 30 and 40 meV, respectively (Supporting Information Section S10). On PC, E_b^T also remains constant within 35−45 meV for 1L-MoS_2. However, for 1L-WS_2 on PC, E_b^T is significantly larger and seems to increase with compressive strain, reaching ∼80 meV (see the inset of Figure 4c). The effect of strain on the binding energies of neutral excitons has been both experimentally and theoretically explored, demonstrating changes of the order of 10 meV/%.[22,35,58,60] However, the effect of strain on the binding energies of trions has been less studied and only in the case of tensile strain experiments.[26,32]

In a first approximation, the binding energies of excitons for an intrinsic 2D semiconductor depend solely on the exciton-reduced mass μ and the screening length ρ for the Coulomb interactions within the material,[4,61−63] which are expected to change under applied strain.[58,64] From first-principles calculations (see the Materials and Methods section), we estimated that a 1.5% biaxial compressive strain can result in an ∼10% increase in the reduced mass for both 1L-MoS_2 and 1L-WS_2 (Supporting Information Section S11). Based on the results in ref 65, we estimated a decrease of ∼4 and ∼2% in the screening lengths of 1L-MoS_2 and 1L-WS_2, respectively, under −1.5% strain. Different models for calculating trion binding energies (see refs 61−63) suggest that increasing μ and decreasing ρ both contribute to an increase in the binding energies of negative trions. However, the estimated increase due to ca. −1.5% strain is found to be modest, less than 3 meV, for both 1L-WS_2 and 1L-MoS_2 (from refs 61,63; see Supporting Information Section S12). Even considering the combined effect of strain and the different dielectric screening from SiO_2 and PC substrates, E_b^T would increase only by as much as ca. 6−7 meV for both 1L-MoS_2 and 1L-WS_2 on PC with respect to Si/SiO_2 at low temperatures (see Supporting Information Section S10). Therefore, considering the sole effect of strain on the intrinsic electronic structure may not suffice to explain the observed large E_b^T. It is important to note that trion binding energies are strongly influenced by carrier concentration,[56,57,60] which can vary substantially between different samples due to charge transfer between the substrate and each specific material. Differences in the intensity ratios between X_T and X_A suggest an increase in electron concentration for samples on PC in comparison to samples on Si/SiO_2. A higher electron concentration can explain the overall increased binding energy for trions in both 1L-MoS_2 and 1L-WS_2 on PC compared to the same materials on Si/SiO_2. However, in 1L-WS_2, E_b^T appears to increase further with induced strain. Interestingly, various works suggest that the doping level of TMDs may change with strain.[66,67] Additionally, a large energy shift for WS_2 trions has been observed under inhomogeneous tensile strain at low temperatures in ref 26, which could arise from strain-induced changes in carrier concentration. In summary, we propose that the further increase in E_b^T for trions with biaxial compressive strain in 1L-WS_2 may arise from a combination of factors, including steady-state substrate effects as well as dynamic strain-induced changes in the intrinsic electronic structure and in the free-carrier concentration of the material. Doping level variations modify the dielectric landscape and result in a renormalization of energy levels, leading to dramatic changes in the overall optical spectrum of the material, and for trion energies, in particular. Therefore, a further understanding of the observed behavior of X_T resonances with strain in 1L-WS_2 requires more sophisticated models than those currently available, capable of

https://doi.org/10.1021/acsami.3c13281
ACS Appl. Mater. Interfaces XXXX, XXX, XXX−XXX

capturing the exact interplay of strain and doping and their impact on the excitonic properties of the material.

CONCLUSIONS

In conclusion, our findings demonstrate an excellent transfer of uniform, biaxial compressive strain (ca. −1.2%) to single-layer materials from the thermal compression of polymer substrates down to 10 K, demonstrated by the large gauge factor values obtained. This strain induces a remarkably large modulation in the exciton energies in single-layer TMDs (up to 160 meV), larger than values obtained in previous compressive strain experiments. The analysis of data over a large temperature range allows us to precisely separate the effects of strain from those of temperature in exciton energies. Furthermore, at low temperatures, we resolve further resonances that we associate with trionic states and study their behavior under biaxial compressive strain. We found a substantial increase in the trion binding energy of 1L-WS_2 on PC at 10 K, which may arise from a combination of substrate-related effects and strain-induced changes in the electronic properties of the material. These findings go beyond the scope of existing models and may require further investigation. The large modulation of exciton resonances in our results holds relevance for applications that require precise manipulation of excitonic states in 2D semiconductors, such as valley selectivity or exciton transport. Moreover, this work demonstrates a simple method to explore the effect of large, uniform compressive strain on low-temperature phenomena in other 2D materials.

MATERIALS AND METHODS

Fabrication of Single-Layer TMD Samples. MoS_2, WS_2, $MoSe_2$, and WSe_2 crystals were mechanically exfoliated onto transparent poly(dimethylsiloxane) (gel film from Gel-Pak) substrates for inspection under an optical Motic BA310 metallurgical microscope. From differential reflectance measurements at room temperature, we were able to identify single-layer TMD flakes. Selected flakes were transferred by a dry-transfer method[44] onto either a 250 μm thick polycarbonate film with size of 6 mm × 6 mm or a 6 mm × 6 mm Si/SiO_2 substrate with a 50 nm oxide layer.

Variable-Temperature Differential Reflectance Measurements. Differential reflectance measurements were performed with a homemade microscope setup based on ref 45. Samples were illuminated by a white light source that was focused on the sample by an infinite corrected 50× objective. Because of the different energy positions of exciton resonances for different materials, two different light sources were used: a SOLIS-3C lamp (400−900 nm) from Thorlabs was used to illuminate the sulfide samples, whereas a halogen lamp (500−1100 nm) from a Motic BA310 microscope was used for selenide samples. A diaphragm is used to reduce the illumination area to a few tens of micrometers on the sample around the measurement spot. A tube lens of focal length f = 20 cm collects the reflected light into an optical fiber. The fiber core (105 μm diameter) determines the diameter of the spot at the sample from which light is collected (~2 μm). The fiber guides the reflected light to a CCS200/M compact spectrometer (Thorlabs). The acquired spectra from the sample and from the substrate are used to calculate the differential reflectance as $DR = (R_{sample} - R_{substrate})/R_{substrate}$, where R_{sample} and $R_{substrate}$ are the reflected light intensities at the sample and substrate, respectively.

The home-built microscope setup described above is located at room temperature above the window of a table-top closed-cycle cryostat (AttoDry 800, Attocube Gmbh) that allows to control the temperature of the sample from 10 to 300 K. The cryostat is equipped with a piezoelectric controller to position the sample under the microscope objective. Reflectance spectroscopy measurements were recorded for both cooling and heating of the samples over a range from 300 to 10 K (at a rate of ~1 K/min) under cryogenic vacuum (<1 × 10^{-6} mbar) for the same locations on sample and substrate. Optical images of the samples during the cooldown or warmup process (see Supporting Information Section S2) allow us to perform spectroscopy at the same location of the sample and substrate at different temperatures. Optical images are inspected to check that no wrinkles or additional defects appear in the single-layer flakes with lowering temperature, suggesting a smooth transfer of strain (see Supporting Information Section S2).

DFT Calculations and Determination of Reduced Masses with Applied Strain. The effective masses are obtained from the electronic structure calculations performed within the density functional theory formalism using the plane-wave pseudopotentials method, as implemented in the pwscf code of the QUANTUM ESPRESSO package.[68] The exchange and correlation potentials were treated within the revised Perdew−Burke−Ernzerhof generalized gradient approximation (PBEsol).[69] Fully relativistic pseudopotentials were considered to include spin−orbit coupling. For all elements, we employed the ultrasoft pseudopotentials obtained from the PS library.[70] We used a Monkhorst−Pack grid of 30 × 30 × 1 points, and the energy cutoff for the plane-wave expansion was 110 Ry. In order to avoid interaction between the periodic images, we introduced a vacuum region of 16 Å. We relax the atomic positions for each strain while keeping the unit cell constant with the BFGS quasi-newton algorithm with a convergence threshold on forces of 1 × 10^{-3} Ry/a_0.

We computed the effective masses at the K point for the two high-symmetry directions $K\Gamma$ and KM of the Brillouin zone, and the averaged value between the two directions is shown in Figure S9. We used two different methods to compute numerically the second derivative of the energy band dispersion. First, we performed a quadratic fit using the three nearest points to the K point spaced by 0.01 $Å^{-1}$ for each direction. Second, we performed a third-order spline interpolation of the same points. The results of both methods were nearly identical, with less than 1% of the difference.

ASSOCIATED CONTENT

Supporting Information

The Supporting Information is available free of charge at https://pubs.acs.org/doi/10.1021/acsami.3c13281.

Further experimental characterization of samples (Raman spectroscopy and optical images), further details on data analysis (parameters from data fittings, resonance position, and intensity determination), gauge factor values for additional samples, a bibliographic comparison of gauge factor values for 1L-TMDs, and DFT estimations of effective masses with strain and binding energy estimations as a function of strain (PDF)

AUTHOR INFORMATION

Corresponding Authors

Andres Castellanos-Gomez − *Materials Science Factory, Instituto de Ciencia de Materiales de Madrid, Consejo Superior de Investigaciones Científicas, 28049 Madrid, Spain;* orcid.org/0000-0002-3384-3405; Email: andres.castellanos@csic.es

M. Reyes Calvo − *Departamento de Física Aplicada, Universidad de Alicante, 03690 Alicante, Spain; Instituto Universitario de Materiales IUMA, Universidad de Alicante, 03690 Alicante, Spain;* orcid.org/0000-0001-5991-2619; Email: reyes.calvo@ua.es

Authors

Eudomar Henríquez-Guerra − *Departamento de Física Aplicada, Universidad de Alicante, 03690 Alicante, Spain; Instituto Universitario de Materiales IUMA, Universidad de Alicante, 03690 Alicante, Spain*

https://doi.org/10.1021/acsami.3c13281
ACS Appl. Mater. Interfaces XXXX, XXX, XXX−XXX

Hao Li − *Materials Science Factory, Instituto de Ciencia de Materiales de Madrid, Consejo Superior de Investigaciones Científicas, 28049 Madrid, Spain*

Pablo Pasqués-Gramage − *Departamento de Física Aplicada, Universidad de Alicante, 03690 Alicante, Spain*

Daniel Gosálbez-Martínez − *Departamento de Física Aplicada, Universidad de Alicante, 03690 Alicante, Spain; Instituto Universitario de Materiales IUMA, Universidad de Alicante, 03690 Alicante, Spain*

Roberto D'Agosta − *Nano-bio Spectroscopy Group and European Theoretical Spectroscopy Facility (ETSF), Departamento de Polímeros y Materiales Avanzados: Física, Química y Tecnología, Universidad del Pais Vasco (UPV/EHU), E-20018 San Sebastián, Spain; IKERBASQUE, Basque Foundation for Science, E-48013 Bilbao, Spain;* orcid.org/0000-0002-0173-0705

Complete contact information is available at: https://pubs.acs.org/10.1021/acsami.3c13281

Funding

The authors acknowledge funding from the Generalitat Valenciana through grants IDIFEDER/2020/005 and IDIFEDER/2021/016 and support from the Plan Gen-T of Excellence for M.R.C (CideGenT2018004) and from the Spanish MCINN through grants PLASTOP PID2020-119124RB-I00, TED2021-131641B-C43, PID2020-115566RB-I00, TED2021-132267B-I00, and PID2020-112811GB-I00. This work was funded by the European Research Council (ERC) under the European Union's Horizon 2020 research and innovation program (grant agreement no. 755655, ERC-StG 2017 project 2D-TOP-SENSE). The authors also acknowledge funding from the EU FLAG-ERA project To2Dox (JTC-2019-009) and the Comunidad de Madrid through the CAIRO-CM project (Y2020/NMT-6661). H.L. acknowledges support from China Scholarship Council (CSC) under grant no. 201907040070. D.G.-M. thanks the Maria Zambrano Program at the University of Alicante founded by the European Union-Next Generation EU. R.D'A. acknowledges support from the Grant No. IT1453- 22 "Grupos Consolidados UPV/EHU del Gobierno Vasco".

Notes

The authors declare no competing financial interest.

REFERENCES

(1) Zheng, W.; Jiang, Y.; Hu, X.; Li, H.; Zeng, Z.; Wang, X.; Pan, A. Light Emission Properties of 2D Transition Metal Dichalcogenides: Fundamentals and Applications. *Adv. Opt. Mater.* **2018**, *6* (21), No. 1800420.

(2) Wang, J.; Verzhbitskiy, I.; Eda, G. Electroluminescent Devices Based on 2D Semiconducting Transition Metal Dichalcogenides. *Adv. Mater.* **2018**, *30* (47), No. 1802687.

(3) Mueller, T.; Malic, E. Exciton Physics and Device Application of Two-Dimensional Transition Metal Dichalcogenide Semiconductors. *npj 2D Mater. Appl.* **2018**, *2* (1), No. 29.

(4) Wang, G.; Chernikov, A.; Glazov, M. M.; Heinz, T. F.; Marie, X.; Amand, T.; Urbaszek, B. *Colloquium*: Excitons in Atomically Thin Transition Metal Dichalcogenides. *Rev. Mod. Phys.* **2018**, *90* (2), No. 021001.

(5) Gao, L. Flexible Device Applications of 2D Semiconductors. *Small* **2017**, *13* (35), No. 1603994.

(6) Chang, H.-Y.; Yang, S.; Lee, J.; Tao, L.; Hwang, W.-S.; Jena, D.; Lu, N.; Akinwande, D. High-Performance, Highly Bendable MoS_2 Transistors with High-K Dielectrics for Flexible Low-Power Systems. *ACS Nano* **2013**, *7* (6), 5446−5452.

(7) Park, S.; Chang, H.-Y.; Rahimi, S.; Lee, A. L.; Tao, L.; Akinwande, D. Transparent Nanoscale Polyimide Gate Dielectric for Highly Flexible Electronics. *Adv. Electron. Mater.* **2018**, *4* (2), No. 1700043.

(8) Ge, R.; Wu, X.; Kim, M.; Shi, J.; Sonde, S.; Tao, L.; Zhang, Y.; Lee, J. C.; Akinwande, D. Atomristor: Nonvolatile Resistance Switching in Atomic Sheets of Transition Metal Dichalcogenides. *Nano Lett.* **2018**, *18* (1), 434−441.

(9) Unuchek, D.; Ciarrocchi, A.; Avsar, A.; Watanabe, K.; Taniguchi, T.; Kis, A. Room-Temperature Electrical Control of Exciton Flux in a van Der Waals Heterostructure. *Nature* **2018**, *560* (7718), 340−344.

(10) Ciarrocchi, A.; Tagarelli, F.; Avsar, A.; Kis, A. Excitonic Devices with van Der Waals Heterostructures: Valleytronics Meets Twistronics. *Nat. Rev. Mater.* **2022**, *7* (6), 449−464.

(11) Quereda, J.; Castellanos-Gomez, A. Excitons Surf the Waves. *Nat. Photonics* **2022**, *16* (3), 179−180.

(12) Wang, G.; Marie, X.; Liu, B. L.; Amand, T.; Robert, C.; Cadiz, F.; Renucci, P.; Urbaszek, B. Control of Exciton Valley Coherence in Transition Metal Dichalcogenide Monolayers. *Phys. Rev. Lett.* **2016**, *117* (18), No. 187401.

(13) Mak, K. F.; He, K.; Shan, J.; Heinz, T. F. Control of Valley Polarization in Monolayer MoS_2 by Optical Helicity. *Nat. Nanotechnol.* **2012**, *7* (8), 494−498.

(14) Sie, E. J.; McIver, J. W.; Lee, Y.-H.; Fu, L.; Kong, J.; Gedik, N. Valley-Selective Optical Stark Effect in Monolayer WS_2. *Nat. Mater.* **2015**, *14* (3), 290−294.

(15) Bertolazzi, S.; Gobbi, M.; Zhao, Y.; Backes, C.; Samorì, P. Molecular Chemistry Approaches for Tuning the Properties of Two-Dimensional Transition Metal Dichalcogenides. *Chem. Soc. Rev.* **2018**, *47* (17), 6845−6888.

(16) Raja, A.; Chaves, A.; Yu, J.; Arefe, G.; Hill, H. M.; Rigosi, A. F.; Berkelbach, T. C.; Nagler, P.; Schüller, C.; Korn, T.; Nuckolls, C.; Hone, J.; Brus, L. E.; Heinz, T. F.; Reichman, D. R.; Chernikov, A. Coulomb Engineering of the Bandgap and Excitons in Two-Dimensional Materials. *Nat. Commun.* **2017**, *8* (1), No. 15251.

(17) Ramos, M.; Marques-Moros, F.; Esteras, D. L.; Mañas-Valero, S.; Henríquez-Guerra, E.; Gadea, M.; Baldoví, J. J.; Canet-Ferrer, J.; Coronado, E.; Calvo, M. R. Photoluminescence Enhancement by Band Alignment Engineering in $MoS_2/FePS_3$ van Der Waals Heterostructures. *ACS Appl. Mater. Interfaces* **2022**, *14* (29), 33482−33490.

(18) Roldán, R.; Castellanos-Gomez, A.; Cappelluti, E.; Guinea, F. Strain Engineering in Semiconducting Two-Dimensional Crystals. *J. Phys.: Condens. Matter* **2015**, *27* (31), No. 313201.

(19) Si, C.; Sun, Z.; Liu, F. Strain Engineering of Graphene: A Review. *Nanoscale* **2016**, *8* (6), 3207−3217.

(20) Dai, Z.; Liu, L.; Zhang, Z. Strain Engineering of 2D Materials: Issues and Opportunities at the Interface. *Adv. Mater.* **2019**, *31* (45), No. 1805417.

(21) Chaves, A.; Azadani, J. G.; Alsalman, H.; da Costa, D. R.; Frisenda, R.; Chaves, A. J.; Song, S. H.; Kim, Y. D.; He, D.; Zhou, J.; Castellanos-Gomez, A.; Peeters, F. M.; Liu, Z.; Hinkle, C. L.; Oh, S.-H.; Ye, P. D.; Koester, S. J.; Lee, Y. H.; Avouris, P.; Wang, X.; Low, T. Bandgap Engineering of Two-Dimensional Semiconductor Materials. *npj 2D Mater. Appl.* **2020**, *4* (1), No. 29.

(22) Zollner, K.; Junior, P. E. F.; Fabian, J. Strain-Tunable Orbital, Spin-Orbit, and Optical Properties of Monolayer Transition-Metal Dichalcogenides. *Phys. Rev. B* **2019**, *100* (19), No. 195126.

(23) Blundo, E.; Felici, M.; Yildirim, T.; Pettinari, G.; Tedeschi, D.; Miriametro, A.; Liu, B.; Ma, W.; Lu, Y.; Polimeni, A. Evidence of the Direct-to-Indirect Band Gap Transition in Strained Two-Dimensional WS_2, MoS_2, and WSe_2. *Phys. Rev. Res.* **2020**, *2* (1), No. 012024.

(24) Conley, H. J.; Wang, B.; Ziegler, J. I.; Haglund, R. F., Jr.; Pantelides, S. T.; Bolotin, K. I. Bandgap Engineering of Strained Monolayer and Bilayer MoS_2. *Nano Lett.* **2013**, *13* (8), 3626−3630.

(25) Carrascoso, F.; Li, H.; Frisenda, R.; Castellanos-Gomez, A. Strain Engineering in Single-, Bi- and Tri-Layer MoS_2, $MoSe_2$, WS_2 and WSe_2. *Nano Res.* **2021**, *14* (6), 1698−1703.
(26) Harats, M. G.; Kirchhof, J. N.; Qiao, M.; Greben, K.; Bolotin, K. I. Dynamics and Efficient Conversion of Excitons to Trions in Non-Uniformly Strained Monolayer WS_2. *Nat. Photonics* **2020**, *14* (5), 324−329.
(27) Carrascoso, F.; Frisenda, R.; Castellanos-Gomez, A. Biaxial versus Uniaxial Strain Tuning of Single-Layer MoS_2. *Nano Mater. Sci.* **2022**, *4* (1), 44−51.
(28) Nayak, A. P.; Pandey, T.; Voiry, D.; Liu, J.; Moran, S. T.; Sharma, A.; Tan, C.; Chen, C.-H.; Li, L.-J.; Chhowalla, M.; Lin, J.-F.; Singh, A. K.; Akinwande, D. Pressure-Dependent Optical and Vibrational Properties of Monolayer Molybdenum Disulfide. *Nano Lett.* **2015**, *15* (1), 346−353.
(29) Lloyd, D.; Liu, X.; Christopher, J. W.; Cantley, L.; Wadehra, A.; Kim, B. L.; Goldberg, B. B.; Swan, A. K.; Bunch, J. S. Band Gap Engineering with Ultralarge Biaxial Strains in Suspended Monolayer MoS_2. *Nano Lett.* **2016**, *16* (9), 5836−5841.
(30) Carrascoso, F.; Li, H.; Obrero-Perez, J. M.; Aparicio, F. J.; Borras, A.; Island, J. O.; Barranco, A.; Castellanos-Gomez, A. Improved Strain Engineering of 2D Materials by Adamantane Plasma Polymer Encapsulation. *npj 2D Mater. Appl.* **2023**, *7* (1), No. 24.
(31) Michail, A.; Anestopoulos, D.; Delikoukos, N.; Parthenios, J.; Grammatikopoulos, S.; Tsirkas, S. A.; Lathiotakis, N. N.; Frank, O.; Filintoglou, K.; Papagelis, K. Biaxial Strain Engineering of CVD and Exfoliated Single- and Bi-Layer MoS_2 Crystals. *2D Mater* **2021**, *8* (1), No. 015023.
(32) Michail, A.; Anestopoulos, D.; Delikoukos, N.; Grammatikopoulos, S.; Tsirkas, S. A.; Lathiotakis, N. N.; Frank, O.; Filintoglou, K.; Parthenios, J.; Papagelis, K. Tuning the Photoluminescence and Raman Response of Single-Layer WS_2 Crystals Using Biaxial Strain. *J. Phys. Chem. C* **2023**, *127* (7), 3506−3515.
(33) Covre, F. S.; Faria, P. E.; Gordo, V. O.; de Brito, C. S.; Zhumagulov, Y. V.; Teodoro, M. D.; Couto, O. D. D.; Misoguti, L.; Pratavieira, S.; Andrade, M. B.; Christianen, P. C. M.; Fabian, J.; Withers, F.; Galvão Gobato, Y. Revealing the Impact of Strain in the Optical Properties of Bubbles in Monolayer $MoSe_2$. *Nanoscale* **2022**, *14* (15), 5758−5768.
(34) Blundo, E.; Junior, P. E. F.; Surrente, A.; Pettinari, G.; Prosnikov, M. A.; Olkowska-Pucko, K.; Zollner, K.; Woźniak, T.; Chaves, A.; Kazimierczuk, T.; Felici, M.; Babiński, A.; Molas, M. R.; Christianen, P. C. M.; Fabian, J.; Polimeni, A. Strain-Induced Exciton Hybridization in WS_2 Monolayers Unveiled by Zeeman-Splitting Measurements. *Phys. Rev. Lett.* **2022**, *129* (6), No. 067402.
(35) Aslan, B.; Deng, M.; Heinz, T. F. Strain Tuning of Excitons in Monolayer WSe 2. *Phys. Rev. B* **2018**, *98* (11), No. 115308.
(36) Zhu, C. R.; Wang, G.; Liu, B. L.; Marie, X.; Qiao, X. F.; Zhang, X.; Wu, X. X.; Fan, H.; Tan, P. H.; Amand, T.; Urbaszek, B. Strain Tuning of Optical Emission Energy and Polarization in Monolayer and Bilayer MoS_2. *Phys. Rev. B* **2013**, *88* (12), No. 121301.
(37) Iff, O.; Tedeschi, D.; Martín-Sánchez, J.; Moczała-Dusanowska, M.; Tongay, S.; Yumigeta, K.; Taboada-Gutiérrez, J.; Savaresi, M.; Rastelli, A.; Alonso-González, P.; Höfling, S.; Trotta, R.; Schneider, C. Strain-Tunable Single Photon Sources in WSe_2 Monolayers. *Nano Lett.* **2019**, *19* (10), 6931−6936.
(38) An, Z.; Soubelet, P.; Zhumagulov, Y.; Zopf, M.; Delhomme, A.; Qian, C.; Faria Junior, P. E.; Fabian, J.; Cao, X.; Yang, J.; Stier, A. V.; Ding, F.; Finley, J. J. Strain Control of Exciton and Trion Spin-Valley Dynamics in Monolayer Transition Metal Dichalcogenides. *Phys. Rev. B* **2023**, *108* (4), No. L041404.
(39) Gant, P.; Huang, P.; Pérez de Lara, D.; Guo, D.; Frisenda, R.; Castellanos-Gomez, A. A Strain Tunable Single-Layer MoS_2 Photodetector. *Mater. Today* **2019**, *27*, 8−13.
(40) Frisenda, R.; Drüppel, M.; Schmidt, R.; Michaelis de Vasconcellos, S.; Perez de Lara, D.; Bratschitsch, R.; Rohlfing, M.; Castellanos-Gomez, A. Biaxial Strain Tuning of the Optical Properties of Single-Layer Transition Metal Dichalcogenides. *npj 2D Mater. Appl.* **2017**, *1* (1), No. 10.
(41) Carrascoso, F.; Lin, D.-Y.; Frisenda, R.; Castellanos-Gomez, A. Biaxial Strain Tuning of Interlayer Excitons in Bilayer MoS_2. *J. Phys. Mater.* **2020**, *3* (1), No. 015003.
(42) Plechinger, G.; Castellanos-Gomez, A.; Buscema, M.; Zant, H. S. J. van. der.; Steele, G. A.; Kuc, A.; Heine, T.; Schüller, C.; Korn, T. Control of Biaxial Strain in Single-Layer Molybdenite Using Local Thermal Expansion of the Substrate. *2D Mater* **2015**, *2* (1), No. 015006.
(43) Huang, S.; Zhang, G.; Fan, F.; Song, C.; Wang, F.; Xing, Q.; Wang, C.; Wu, H.; Yan, H. Strain-Tunable van Der Waals Interactions in Few-Layer Black Phosphorus. *Nat. Commun.* **2019**, *10* (1), No. 2447.
(44) Castellanos-Gomez, A.; Buscema, M.; Molenaar, R.; Singh, V.; Janssen, L.; van der Zant, H. S. J.; Steele, G. A. Deterministic Transfer of Two-Dimensional Materials by All-Dry Viscoelastic Stamping. *2D Mater* **2014**, *1* (1), No. 011002.
(45) Frisenda, R.; Niu, Y.; Gant, P.; Molina-Mendoza, A. J.; Schmidt, R.; Bratschitsch, R.; Liu, J.; Fu, L.; Dumcenco, D.; Kis, A.; Lara, D. P. D.; Castellanos-Gomez, A. Micro-Reflectance and Transmittance Spectroscopy: A Versatile and Powerful Tool to Characterize 2D Materials. *J. Phys. D: Appl. Phys.* **2017**, *50* (7), No. 074002.
(46) Roy, R.; Agrawal, D. K.; McKinstry, H. A. Very Low Thermal Expansion Coefficient Materials. *Annu. Rev. Mater. Sci.* **1989**, *19* (1), 59−81.
(47) Li, Z.; Chen, X.; Zhang, C.; Baer, E.; Langhe, D.; Ponting, M.; Brubaker, M.; Hosking, T.; Li, R.; Fukuto, M.; Zhu, L. High Dielectric Constant Polycarbonate/Nylon Multilayer Films Capacitors with Self-Healing Capability. *ACS Appl. Polym. Mater.* **2019**, *1* (4), 867−875.
(48) Anderson, W. E. *Measurements on Insulating Materials at Cryogenic Temperatures*; Final Report National Bureau of Standards: Washington, DC, Electrosystems Div, 1980.
(49) Robertson, J. High Dielectric Constant Gate Oxides for Metal Oxide Si Transistors. *Rep. Prog. Phys.* **2006**, *69* (2), 327.
(50) Hsu, W.-T.; Quan, J.; Wang, C.-Y.; Lu, L.-S.; Campbell, M.; Chang, W.-H.; Li, L.-J.; Li, X.; Shih, C.-K. Dielectric Impact on Exciton Binding Energy and Quasiparticle Bandgap in Monolayer WS_2 and WSe_2. *2D Mater* **2019**, *6* (2), No. 025028.
(51) Baschek, G.; Hartwig, G. Parameters Influencing the Thermal Expansion of Polymers and Fibre Composites. *Cryogenics* **1998**, *38* (1), 99−103.
(52) O'Donnell, K. P.; Chen, X. Temperature Dependence of Semiconductor Band Gaps. *Appl. Phys. Lett.* **1991**, *58* (25), 2924−2926.
(53) Tongay, S.; Zhou, J.; Ataca, C.; Lo, K.; Matthews, T. S.; Li, J.; Grossman, J. C.; Wu, J. Thermally Driven Crossover from Indirect toward Direct Bandgap in 2D Semiconductors: $MoSe_2$ versus MoS_2. *Nano Lett.* **2012**, *12* (11), 5576−5580.
(54) Chernikov, A.; Berkelbach, T. C.; Hill, H. M.; Rigosi, A.; Li, Y.; Aslan, B.; Reichman, D. R.; Hybertsen, M. S.; Heinz, T. F. Exciton Binding Energy and Nonhydrogenic Rydberg Series in Monolayer WS_2. *Phys. Rev. Lett.* **2014**, *113* (7), No. 076802.
(55) Courtade, E.; Semina, M.; Manca, M.; Glazov, M. M.; Robert, C.; Cadiz, F.; Wang, G.; Taniguchi, T.; Watanabe, K.; Pierre, M.; Escoffier, W.; Ivchenko, E. L.; Renucci, P.; Marie, X.; Amand, T.; Urbaszek, B. Charged Excitons in Monolayer WSe 2: Experiment and Theory. *Phys. Rev. B* **2017**, *96* (8), No. 085302.
(56) Chernikov, A.; van der Zande, A. M.; Hill, H. M.; Rigosi, A. F.; Velauthapillai, A.; Hone, J.; Heinz, T. F. Electrical Tuning of Exciton Binding Energies in Monolayer WS_2. *Phys. Rev. Lett.* **2015**, *115* (12), No. 126802.
(57) Mak, K. F.; He, K.; Lee, C.; Lee, G. H.; Hone, J.; Heinz, T. F.; Shan, J. Tightly Bound Trions in Monolayer MoS_2. *Nat. Mater.* **2013**, *12* (3), 207−211.
(58) Defo, R. K.; Fang, S.; Shirodkar, S. N.; Tritsaris, G. A.; Dimoulas, A.; Kaxiras, E. Strain Dependence of Band Gaps and Exciton Energies in Pure and Mixed Transition-Metal Dichalcogenides. *Phys. Rev. B* **2016**, *94* (15), No. 155310.

https://doi.org/10.1021/acsami.3c13281
ACS Appl. Mater. Interfaces XXXX, XXX, XXX−XXX

(59) Mouri, S.; Miyauchi, Y.; Matsuda, K. Tunable Photoluminescence of Monolayer MoS_2 via Chemical Doping. *Nano Lett.* **2013**, *13* (12), 5944−5948.
(60) Luo, Z.; Jia, H.; Lv, L.; Wang, Q.; Yan, X. Gate-Tunable Trion Binding Energy in Monolayer MoS_2 with Plasmonic Superlattice. *Nanoscale* **2020**, *12* (34), 17754−17761.
(61) Berkelbach, T. C.; Hybertsen, M. S.; Reichman, D. R. Theory of Neutral and Charged Excitons in Monolayer Transition Metal Dichalcogenides. *Phys. Rev. B* **2013**, *88* (4), No. 045318.
(62) Thilagam, A. Exciton Complexes in Low Dimensional Transition Metal Dichalcogenides. *J. Appl. Phys.* **2014**, *116* (5), No. 053523.
(63) Szyniszewski, M.; Mostaani, E.; Drummond, N. D.; Fal'ko, V. I. Binding Energies of Trions and Biexcitons in Two-Dimensional Semiconductors from Diffusion Quantum Monte Carlo Calculations. *Phys. Rev. B* **2017**, *95* (8), No. 081301.
(64) Shi, H.; Pan, H.; Zhang, Y.-W.; Yakobson, B. I. Quasiparticle Band Structures and Optical Properties of Strained Monolayer MoS_2 and WS_2. *Phys. Rev. B* **2013**, *87* (15), No. 155304.
(65) Wang, L.; Kutana, A.; Yakobson, B. I. Many-Body and Spin-Orbit Effects on Direct-Indirect Band Gap Transition of Strained Monolayer MoS_2 and WS_2. *Ann. Phys.* **2014**, *526* (9−10), L7−L12.
(66) Sensoy, M. G.; Vinichenko, D.; Chen, W.; Friend, C. M.; Kaxiras, E. Strain Effects on the Behavior of Isolated and Paired Sulfur Vacancy Defects in Monolayer MoS_2. *Phys. Rev. B* **2017**, *95* (1), No. 014106.
(67) Zeng, J.; Liu, G.; Han, Y.; Luo, W.; Wu, M.; Xu, B.; Ouyang, C. Effects of Strain and Electric Field on Molecular Doping in MoSSe. *ACS Omega* **2021**, *6* (22), 14639−14647.
(68) Giannozzi, P.; Baroni, S.; Bonini, N.; Calandra, M.; Car, R.; Cavazzoni, C.; Ceresoli, D.; Chiarotti, G. L.; Cococcioni, M.; Dabo, I.; Corso, A. D.; Gironcoli, S. de.; Fabris, S.; Fratesi, G.; Gebauer, R.; Gerstmann, U.; Gougoussis, C.; Kokalj, A.; Lazzeri, M.; Martin-Samos, L.; Marzari, N.; Mauri, F.; Mazzarello, R.; Paolini, S.; Pasquarello, A.; Paulatto, L.; Sbraccia, C.; Scandolo, S.; Sclauzero, G.; Seitsonen, A. P.; Smogunov, A.; Umari, P.; Wentzcovitch, R. M. QUANTUM ESPRESSO: A Modular and Open-Source Software Project for Quantum Simulations of Materials. *J. Phys.: Condens. Matter* **2009**, *21* (39), No. 395502.
(69) Perdew, J. P.; Ruzsinszky, A.; Csonka, G. I.; Vydrov, O. A.; Scuseria, G. E.; Constantin, L. A.; Zhou, X.; Burke, K. Restoring the Density-Gradient Expansion for Exchange in Solids and Surfaces. *Phys. Rev. Lett.* **2008**, *100* (13), No. 136406.
(70) Dal Corso, A. Pseudopotentials Periodic Table: From H to Pu. *Comput. Mater. Sci.* **2014**, *95*, 337−350.

https://doi.org/10.1021/acsami.3c13281
ACS Appl. Mater. Interfaces XXXX, XXX, XXX−XXX